J. Fluid Mech. (1981), *vol.* 102, *pp.* 279–299
Printed in Great Britain

Oscillatory flow around disks and through orifices

By B. DE BERNARDINIS,† J. M. R. GRAHAM AND K. H. PARKER

Physiological Flow Studies Unit, Department of Aeronautics, Imperial College, London

(Received 27 February 1980)

Two examples of unsteady, axisymmetric, separated flows are studied: unbounded oscillatory flow around a disk and bounded oscillatory flow through a sharp-edged orifice. Calculations are made assuming that the flow is inviscid and that the shed vortex sheets can be represented by sequences of discrete vortex rings. The solid bodies (i.e. the disk or the orifice and bounding tube) are also represented by a distribution of bound discrete vortex rings whose strengths are chosen to satisfy the Neumann or zero normal velocity boundary condition.

The results of flow visualization experiments and, for the orifice, pressure drop measurements are also reported. In general, the gross properties of the flows are predicted accurately.

1. Introduction

The modelling of two-dimensional free shear layers by discrete vortices has been used by many authors since it was proposed by Rosenhead (1931). Fink & Soh (1974) and Clements & Maull (1975) give extensive reviews of the applications of this model as well as discussions of its limitations. More recently it has been used by Evans & Bloor (1976) to study impulsive flow through a sharp-edged orifice; by Sarpkaya & Schoaff (1979) to study the wake behind an impulsively started circular cylinder; and by Graham (1980) to study the force on sharp-edged cylinders in oscillatory flow.

The extension of this model to axisymmetric flows is obvious but not trivial. Among the problems which arise are: a much more complicated interaction between vortices; the possibility of vortex stretching; and the existence of the self-induced velocity of a vortex ring. Davies & Hardin (1974) used the discrete vortex method to calculate the initial behaviour of an impulsively started circular jet.

Very few other axisymmetric calculations have been published. Calculations have been made to predict the flow in an axisymmetric piston cavity during a full cycle of a four-stroke engine which was compared with some results using flow visualization in water (Ashurst 1979).

Flow visualization of vortex rings formed by oscillatory flow in and out of an open-ended tube have also been obtained by Knott & Mackley (1980) in their study of the energy losses of a wave-energy device. However, no specific vortex ring calculations have yet been carried out for this case.

In this paper we explore the theoretical basis of the axisymmetric, discrete vortex model. We then apply it; calculating first the unbounded oscillatory flow around a

† On leave from Facoltà di Ingegneria, Università di Genova.

0022-1120/81/4656-2950 $02.00

disk. This is the axisymmetric analogue of two-dimensional oscillatory flow around a flat plate; a problem which has received considerable attention because of its relevance to wave loading and other fluid–structural interactions (see, for example, Graham 1980). In order to check some of the predictions of our calculations, we performed flow visualization experiments with an oscillating disk.

For our second application of the model, we calculate oscillatory flow through an orifice in a circular tube. This flow, being bounded, is fundamentally different from the external flows which have been studied using this model.

Research on unsteady flows through constricted tubes has been stimulated by the physiological importance of these flows. Caro, Fitzgerald & Schroter (1971) and Fry (1973) have suggested that hydrodynamic factors may influence the genesis and subsequent development of atherosclerosis. This is a disease involving the development of fatty deposits in the artery wall. In its advanced stages, these deposits cause a progressive occlusion of the artery and can strongly influence the flow of blood through the affected artery (Young 1979).

A better understanding of the complex fluid mechanics involved could lead to better methods for the detection of arterial stenoses. Auscultation, the oldest and most common means of detection, relies upon the detection of sounds generated by the flow through the stenosis. These sounds are generated by both pressure fluctuations in the fluid and vibrations of the elastic arterial walls (see, for example, Tomm 1977).

The prediction of the pressure drop across a stenosis has been the subject of several studies. Young & Tsai (1973*a*, *b*) developed an equation for the unsteady pressure drop which used coefficients which were determined from steady flow experiments. The predicted peak pressure drop was always found to be lower than that found experimentally. Clark (1976*a*, *b*) introduced an apparent friction factor which took into account changes in momentum flux due to the development of the boundary layer. The prediction of both the pressure drop and the pressure recovery away from the constriction were in good agreement with steady and oscillatory flow measurements.

Mates *et al.* (1978) found that flow separation occurs in relatively mild constrictions and suggest that an appreciable portion of the pressure drop is a result of energy dissipation in the recirculation regions. They also observed that for severe stenoses the total pressure drop was primarily dependent on the minimum area and was relatively independent of the detailed geometry of the stenosis – a sharp-edged orifice and a long, smooth stenosis behaved similarly. Because of this observation and because the problem of separation from a smooth surface is generally unsolved, even for the simple case of steady flow, we have restricted the theoretical and experimental investigations presented here to sharp-edged constrictions where separation can be confidently assumed to occur, and its position is fixed.

2. Mathematical description of the model

We assume initially that we are modelling flows at very high Reynolds numbers. Later the consequences for more moderate Reynolds-number flows in pipes will be considered. Therefore, the flow fields we are considering generally contain large-scale structures in which viscosity is relatively unimportant. The formation of these large-scale structures, however, depends upon the existence of free shear layers resulting

from flow separation. A common reason for flow separation is the presence in the boundaries of regions of high curvature relative to the local boundary-layer thickness. In these regions, the flow is unable to negotiate the curve and separates forming a free shear layer of thickness comparable to that of the boundary layer. Thus, the effects of viscosity are important in the formation of the large-scale structures but are confined to a small region close to the boundaries.

In the limit of infinite Reynolds number, we assume that a bound vortex sheet exists on the boundary and is shed at the point of separation as a free vortex sheet which is convected with the local velocity. In this limit, the problem becomes an inviscid one which can be analysed using potential flow theory with the effects of viscosity being replaced by a Kutta–Joukowski condition at the point of separation. The problem can be divided into three parts: (*a*) the potential-flow solution, (*b*) the inviscid flow separation and (*c*) the evolution of the free vortex sheet.

(*a*) *Potential-flow solution*

The governing equation for an inviscid flow is the Laplace equation

$$\nabla^2\phi = 0, \tag{1}$$

where ϕ is the velocity potential, $\mathbf{v} = \nabla\phi$. The boundary condition is

$$\mathbf{v}.\mathbf{n}|_S = \mathscr{F}(\mathbf{x}, t), \tag{2}$$

where S is the boundary of the flow defined by the equation

$$F(\mathbf{x}, t) = 0, \tag{3}$$

$\mathbf{n}$ is the unit normal to S defined as positive on the wetted surface, and $\mathscr{F}(\mathbf{x}, t)$ is a function which is determined by the imposed boundary conditions. For stationary boundaries without sources or sinks, $\mathscr{F} = 0$.

The pressure is given by the unsteady Bernoulli equation

$$p/\rho + \tfrac{1}{2}\mathbf{v}.\mathbf{v} + \frac{\partial\phi}{\partial t} = \xi(t), \tag{4}$$

where p is the pressure, ρ is the density which is assumed to be constant, and $\xi(t)$ is an instantaneous constant throughout the flow.

Since the problem is linear, we can express the velocity

$$\mathbf{v} = \mathbf{v}_\infty + \mathbf{v}_b + \mathbf{v}_v, \tag{5}$$

where $\mathbf{v}_\infty(t)$ is the velocity imposed at infinity, $\mathbf{v}_b(\mathbf{x}, t)$ is the irrotational disturbance velocity due to the presence of the boundaries, and $\mathbf{v}_v(\mathbf{x}, t)$ is the velocity due to the singularities in the flow field. If $\phi_b(\mathbf{x}, t)$ is the potential of the disturbance velocity, $\mathbf{v}_b$, then equation (1) becomes

$$\nabla^2\phi_b = 0 \tag{6}$$

and the boundary condition, equation (2), becomes

$$\nabla\phi_b.\mathbf{n}|_S = \mathscr{F} - \mathbf{v}_\infty.\mathbf{n}|_S - \mathbf{v}_v.\mathbf{n}|_S \equiv \mathscr{T}(\mathbf{x}, t). \tag{7}$$

A boundary integral method has been used to solve equations (6) and (7). In this method, singularities are distributed over the boundary and their strengths are

calculated so that the prescribed normal velocity boundary condition is satisfied. In a previous application of this method, Chaplin (1964) used a distribution of vortex rings to simulate the boundary in his study of a steady axisymmetric flow through a shrouded impulse disk. We have also found a distribution of vortex rings to be the most convenient in our calculations.

Restricting our analysis, now and in the rest of this paper, to axisymmetric flows where $\mathbf{x} = (x, \sigma)$ and $\mathbf{v} = (u, v)$, the boundary condition (7) becomes

$$\frac{1}{4\pi}\int_S \gamma(x', \sigma', t)\,[\tilde{u}F_x + \tilde{v}F_\sigma]\,dl' = \mathscr{T}(x, \sigma, t), \tag{8}$$

where $\gamma(x, \sigma, t)$ is the strength of the distributed vorticity. $(\tilde{u}, \tilde{v})$ is the velocity at (x, σ) due to a unit vortex ring at (x', σ'). This velocity can be obtained from Lamb's (1957) solution

$$\tilde{u}(x, \sigma; x', \sigma') = \frac{1}{2\pi[(x-x')^2+(\sigma+\sigma')^2]^{\frac{1}{2}}}\left\{\mathscr{K}(m) - \frac{(x-x')^2+\sigma^2-\sigma'^2}{(x-x')^2+(\sigma-\sigma')^2}\mathscr{E}(m)\right\}, \tag{9}$$

$$\tilde{v}(x, \sigma; x', \sigma') = \frac{-(x-x')}{2\pi\sigma[(x-x')^2+(\sigma+\sigma')^2]^{\frac{1}{2}}}\left\{\mathscr{K}(m) - \frac{(x-x')^2+\sigma^2+\sigma'^2}{(x-x')^2+(\sigma-\sigma')^2}\mathscr{E}(m)\right\}, \tag{10}$$

where $\mathscr{K}(m)$ and $\mathscr{E}(m)$ are the complete elliptic integrals of the first and second kind with the argument

$$m = \frac{4\sigma\sigma'}{(x-x')^2+(\sigma+\sigma')^2}. \tag{11}$$

Equation (8) is a Fredholm equation of the first kind. An approximate solution can be obtained by approximating the boundary by a polygonal contour composed of N conical segments δS_j. The integrand between successive midpoints of the segments is assumed to be constant and equal to its value at the junction. The result is a set of simultaneous equations

$$\sum_{j=1}^{N} \Gamma_j\,[\tilde{v}(x_i, \sigma_i; x_j, \sigma_j)\cos\beta_i - \tilde{u}(x_i, \sigma_i; x_j, \sigma_j)\sin\beta_i] = \mathscr{T}_i \quad (i = 1, 2, \ldots, N), \tag{12}$$

which is equivalent to approximating the continuous distribution of vorticity, γ, by a set of bound vortex rings of strength

$$\Gamma_j = \bar{\gamma}_j \delta S_j. \tag{13}$$

Equation (12) can be written in matrix form

$$\mathbf{A\Gamma} = \mathbf{G}, \tag{14}$$

which has the solution

$$\mathbf{\Gamma} = \mathbf{A}^{-1}\mathbf{G}. \tag{15}$$

Note that the matrix $\mathbf{A}$ and hence $\mathbf{A}^{-1}$ depends only upon the geometry of the boundary.

The tangential velocity at the boundary, $v_\tau = \mathbf{v}.\boldsymbol{\tau}$, is given at the midpoints of each element by the equation

$$v_{\tau i} = \sum_{j=1}^{N} \Gamma_j\,[\tilde{v}(x_i, \sigma_i; x_j, \sigma_j)\sin\beta_i + \tilde{u}(x_i, \sigma_i; x_j, \sigma_j)\cos\beta_i] + (\mathbf{v}_\infty.\boldsymbol{\tau})_i + (\mathbf{v}_v.\boldsymbol{\tau})_i + \tfrac{1}{2}\gamma_i \quad (i = 1, 2, \ldots, N). \tag{16}$$

The last term is the tangential velocity due to the local surface distribution of vorticity. In matrix notation and using equation (15)

$$\mathbf{V}_\tau = \mathbf{B}\mathbf{A}^{-1}\mathbf{G} + \mathbf{V}_\infty + \mathbf{V}_v + \mathbf{V}. \tag{17}$$

Again, the matrix $\mathbf{B}\mathbf{A}^{-1}$ depends only upon the geometry of the boundary.

The accuracy of this method depends upon the number and distribution of the elements (Smith & Pierce 1958; Hess & Smith 1966). Particular care must be taken around geometrical singularities in the boundaries. As d, the distance along the boundary from the singularity, decreases, Δ, the size of the element, should decrease. Using results from the next section, it can be seen that $\Delta \propto d^{1/\lambda}$, where $\lambda = 2-\delta/\pi$ and δ is the internal angle of the singularity.

This method for calculating the potential flow is simpler but less accurate for a given number of elements than those published by Chaplin (1964), Smith & Pierce (1958) and Hess & Smith (1966). In order to check if the loss of accuracy was acceptable, we recalculated all of the axisymmetric examples given in these papers and concluded that the slight loss of accuracy was more than compensated for by the relative simplicity of our method.

(*b*) *Inviscid vortex shedding*

Prandtl (1924) proposed a similarity law for the vortex shed from the apex of semi-infinite wedge in two-dimensional starting flow. Anton (1939) and Wedermeyer (1964) derived a solution for the case of zero wedge angle. In the axisymmetric case in which the vortex sheet rolls up to form a vortex ring, no such similarity law has been found (Didden 1979). However, Saffman (1978) has proposed that the two-dimensional law should be valid for short times; that is, for times small enough so that the characteristic length scale of the shedding is small compared to the radius of the singularity. He found reasonable agreement with experiments in which the ejection time was short.

We assume that the vortex shedding in our axisymmetric problem is governed by the flow characteristics near to the geometrical singularity in the boundary. We further assume that the region of influence is small compared to the radius of the singularity so that we can take the shedding to be locally two-dimensional. Graham (1977) has discussed two-dimensional vortex shedding from an infinite sharp edge in detail and this section follows his results closely.

If the flow past an edge of internal angle δ does not separate, then in the vicinity of the edge the flow can be described by the complex velocity

$$W(z) = \frac{2U}{\lambda} Z^{(2-\lambda)/\lambda} + i\frac{V}{\lambda} Z^{(1-\lambda)/\lambda}, \tag{18}$$

where U and V are real constants describing the symmetrical and asymmetrical (relative to the median plane of the wedge) parts of the flow and $\lambda = 2-\delta/\pi$. The part of the flow due to the asymmetric velocity, V, is singular at the edge and gives rise to the flow separation.

Giesing (1969) has derived a relationship between V and the properties of the shed vortex sheet. Briefly, he assumes that the element of vortex sheet shed in a small time interval δt is straight, of length δS and of uniform strength γ. The wedge is

transformed into a plane surface by the transformation $z = \zeta^\lambda$ and the Kutta–Joukowski condition of finite velocity at $\zeta = 0$ is applied. This yields a relationship between V and δS

$$V = \frac{\gamma\lambda \sin(\pi/\lambda)}{\pi(\lambda - 1)} \delta S^{(\lambda-1)/\lambda}. \tag{19}$$

He also shows that when $\delta \neq 0$, the free vortex sheet must leave the edge tangentially to the wetted surface (i.e. at an angle $-\frac{1}{2}\delta$) with the convection velocity

$$\frac{\delta S}{\delta t} = \tfrac{1}{2}\gamma. \tag{20}$$

This means that a stagnation point must exist on the unwetted side of the edge. Combining equations (19) and (20), we see that

$$\delta S = C L_V, \tag{21}$$

where C depends only upon the wedge angle, δ,

$$C = \left[\frac{\pi(\lambda - 1)}{2\lambda \sin(\pi/\lambda)}\right]^{\lambda/(2\lambda-1)} \tag{22}$$

and L_V is a characteristic length associated with the asymmetric part of the local flow

$$L_V = [V \delta t]^{\lambda/(2\lambda-1)}. \tag{23}$$

The total circulation, $\Gamma = \gamma \delta S$, of the element shed in time δt is by equation (21) and (23)

$$\Gamma = \frac{2C^2 L_V^2}{\delta t}. \tag{24}$$

When the integral method of the previous section is used, the asymmetric edge velocity, V, can be expressed in terms of the velocities Q_w and Q_u at the midpoints of the conical segments on the wetted and unwetted side of the edge,

$$V = \frac{\lambda \Delta_e^{(\lambda-1)/\lambda}}{2^{(2\lambda-1)/\lambda}} (Q_w + Q_u), \tag{25}$$

where Δ_e is the length of the edge element.

For the special case, $\delta = 0$, it is obvious that there does not have to be a stagnation point on the unwetted surface of the wedge. Thus, the convective velocity at the edge depends upon U, the symmetrical velocity component. However, experimental (Fage & Johansen 1928) and computed (Graham 1977) results indicate that the velocity on the unwetted side of a flat edge is generally small. That is, U is only slightly greater than $\frac{1}{2}\gamma$ and consequently it can be assumed empirically that the convective velocity at the edge is also equal to $\frac{1}{2}\gamma$ for $\delta = 0$.

Finally, when considering the motion of a fluid starting from rest special care must be taken in the representation of the first element of vortex sheet which is shed. This first element, unlike succeeding elements, will roll up into a tight spiral. Brown & Michael (1955) suggested that this element could be represented by a vortex located at the centre of the growing spiral joined to the edge by a cut representing the sheet. Thus, a concentrated vortex is first shed followed by continuous shedding of vortex elements representing the subsequent vortex sheet. This representation is analogous

to that used by Mangler & Smith (1956) to represent vortex sheets above slender wings.

Using the above-described transformation and the Kutta–Joukowski condition in the transformed plane, the position Z_0 and strength Γ_0 of the first shed vortex can be calculated. For an attached flow with $U = 0$ and $V = \hat{V}t^b$

$$Z_0 = K^{\lambda/(2\lambda-1)} L_V e^{i\theta}, \tag{26}$$

$$\Gamma_0 = \frac{2\pi K^{1/(2\lambda-1)} L_V^2}{\sqrt{\lambda}\, \delta t_0}, \tag{27}$$

where

$$K = \frac{(4-\lambda)^{\frac{1}{2}}(\lambda-1)(2\lambda-1)}{2\lambda^2(3b\lambda+\lambda+1)} \quad \text{and} \quad \theta = -\lambda \cos^{-1}(\tfrac{1}{2}\lambda^{\frac{1}{2}}). \tag{28}$$

The total circulation of the first element calculated by equation (27) is similar to that which would be calculated by equation (24). However, the shedding angle θ of the first element can be dramatically different from the value $-\frac{1}{2}\delta$ for succeeding elements. In the extreme case of $\delta = 0$, the first vortex is shed at an angle of $-\frac{1}{2}\pi$ (measured relative to the plane of the edge) while succeeding vortices are shed at an angle of 0. We found that the proper placement of the initial vortex could be important when calculating the detailed nature of a starting flow.

(*c*) *Vortex sheet evolution*

The final part of our problem is to describe the evolution of the vortex sheet once it has been shed. We have used the 'point vortex' representation which has been studied extensively since it was proposed by Rosenhead (1931) (see reviews by Fink & Soh 1974 and Clements & Maull 1975). Moore (1974) has discussed the difficulties and inherent limitations of this method and has succeeded in describing the evolution of an elliptically loaded vortex sheet. Clements (1973) and Sarpkaya (1975) have used the point vortex model to describe the two-dimensional free shear layer shed from sharp-edged bodies. Davies & Hardin (1974) used the method to model an axisymmetric starting jet. They found qualitative agreement between their calculations and experiments.

In our model, the vortex sheet is represented by a number of vortex rings whose initial strengths and positions are determined by the shedding discussed in the previous section. Each vortex ring has an infinitesimally small core with a finite circulation which is equal to the circulation of the vortex sheet element shed in the time δt. That is, the strength of the nth vortex $\Gamma_n = \gamma_n \delta S_n$ which, using equation (20), can be written

$$\Gamma_n = 2\frac{\delta S_n^2}{\delta t_n}. \tag{29}$$

The initial position of the nth vortex is taken as the midpoint of the element of vortex sheet shed during the interval δt_n. As pointed out by Graham (1977), this initial location leads to a small violation of the Kutta–Joukowski condition, but to a more accurate description of the convection of the element.

There are basic differences between the behaviour of a two-dimensional and an axisymmetric vortex sheet. Fink & Soh (1974) have shown that the point vortex representation of a two-dimensional vortex sheet produces a logarithmic error in the

self-induced velocity field unless the point vortex remains in the centre of the element which it represents. Sarpkaya (1975) claims that this error is relatively unimportant compared to other errors inherent in the method.

For an axisymmetric vortex sheet, there is an additional contribution to the self-induced velocity arising from the circular symmetry. We analyse this contribution by calculating the self-induced velocity at the midpoint $(\bar{x}, \bar{\sigma})$ of a short, straight conical section of an axisymmetric vortex sheet of uniform strength $\bar{\gamma}$ and length $2S_0$

$$u^*(\bar{x}, \bar{\sigma}) = \frac{\bar{\gamma}}{4\pi}\int_{-S_0}^{S_0} \tilde{u}(\bar{x}, \bar{\sigma}; x', \sigma')\, dS', \tag{30}$$

$$v^*(\bar{x}, \bar{\sigma}) = \frac{\bar{\gamma}}{4\pi}\int_{-S_0}^{S_0} \tilde{v}(\bar{x}, \bar{\sigma}; x', \sigma')\, dS', \tag{31}$$

where $\tilde{u}$ and $\tilde{v}$ are defined in equations (9) and (10).

These integrals are improper for $(x', \sigma') = (\bar{x}, \bar{\sigma})$. In order to overcome this difficulty, we define the variables $\eta = S/\bar{\sigma}$ and $\alpha = \tan^{-1}\{(\sigma' - \bar{\sigma})/(x' - \bar{x})\}$, substitute them into equations (9) and (10) and obtain series expansions for the velocities for $\eta \to 0$. Substituting these series into equations (30) and (31) and integrating term by term, we obtain the expansions for the self-induced velocity at the midpoint,

$$u^*(\eta_0, \alpha) = \frac{\bar{\gamma}}{4\pi}\eta_0\left\{\left[1 + \tfrac{1}{48}(4\sin^2\alpha - 3)\eta_0^2\right]\ln\frac{64}{\eta_0^2} + \left[2\sin^2\alpha + \tfrac{1}{72}(9 - 23\sin^2\alpha + 6\sin^4\alpha)\eta_0^2\right]\right\} + O(\eta_0^3), \tag{32}$$

$$v^*(\eta_0, \alpha) = -\frac{\bar{\gamma}}{4\pi}\sin\alpha\cos\alpha\,\eta_0\left\{\frac{\eta_0^2}{8}\ln\frac{64}{\eta_0^2} + \left[2 - \frac{\eta_0^2}{24}(9 - 2\sin^2\alpha)\right]\right\} + O(\eta_0^3). \tag{33}$$

We note that, if a vortex sheet of defined strength $\gamma(S)$ is represented by a sequence of conical elements of vortex sheet of locally uniform strength, the self-induced velocity of each element decreases as $\eta_0 \ln \eta_0$ as the number of elements is increased, thus decreasing η_0.

In the point-vortex method we approximate each element of vortex sheet by a vortex ring with an infinitesimally small core. Theoretically, the self-induced velocity of a vortex ring of constant circulation increases weakly to infinity as its core radius decreases to zero. However, these vortex rings are being used to represent small elements of vortex sheet whose self-induced velocity decreases to zero as the element length goes to zero. In practice there is a small self-induced velocity for a finite-length element which we neglect to leading order in the vortex-ring representation. It is best to consider our vortices not as physical vortex rings but as a discrete numerical representation of a continuous vorticity distribution.

Practically, the above analysis provides a strong condition on the length of the shed element δS and hence the time step δt. We require that the neglected self-induced velocity of the element be small compared to the characteristic convection velocity, U^*, of the element at the shedding edge $L_V/\delta t$. Taking the leading-order term from equations (32) and (33) for $\alpha = \frac{1}{2}\pi$, we obtain the ratio

$$\frac{U^*\delta t}{L_V} \simeq \frac{C^2 L_V}{4\pi\bar{\sigma}}\left[\ln\frac{256\bar{\sigma}^2}{C^2 L_V^2} + 2\right]. \tag{34}$$

This requires that $(L_V/\bar{\sigma})\ln[L_V/\bar{\sigma}]$ be small whereas the assumption in subsection (*b*) that the shedding was locally two-dimensional required only that $L_V/\bar{\sigma}$ be small.

As discussed in the previous section, the first vortex which is shed must be treated differently from succeeding vortices because it represents a rolled-up element of vortex sheet rather than a short element of essentially straight vortex sheet. If we assume that the inner part of the vortex sheet represented by the first vortex is described by a Kaden-type spiral, then we can obtain an estimate for the inner core radius (Saffman 1978)

$$a \simeq \left\{\left[\frac{1{\cdot}9K^{1/(2\lambda-1)}}{\sqrt{\lambda}}\right]^{\lambda} L_V\right\}^{(1+b)/(2\lambda b+1)} = \{C_a L_V\}^{(1+b)/(2\lambda b+1)}. \tag{35}$$

The self-induced velocity U_0^* of a vortex ring of radius σ_0 and core radius a is given by Kelvin's formula (Lamb 1957) which yields, using equations (28) and (35) with $b = 0$,

$$\frac{U_0^*\,\delta t}{L_V} = \frac{K^{1/(2\lambda-1)} L_V}{2\sqrt{\lambda}\,\sigma_0}\left[\ln\frac{8\sigma_0}{C_a L_V} - \tfrac{1}{4}\right]. \tag{36}$$

Again we see that neglecting the self-induced velocity of this vortex introduces an error of order $(L_V/\sigma_0)\ln[L_V/\sigma_0]$.

We conclude this section with a discussion of the amalgamation of vortices. Moore (1974) has pointed out that in the calculation of the rolling up of a vortex sheet the representation of the inner core by a single vortex reduces numerical disturbances. This representation has already been used in our modelling of the first element of the vortex sheet. Graham (1977) has suggested that the continuing two-dimensional rolling-up process could also be modelled by successively amalgamating the vortices representing the core. If two vortices do amalgamate, the strength and position of the resultant vortex can be determined by conservation of the total circulation and the total impulse (Lamb 1957).

In the case of axisymmetric flow, however, such a representation of the rolling-up process may not be appropriate, unless a proper calculation of the self-induced velocity of the resultant vortex ring can be obtained. Such a calculation has not been attempted. Instead, we assume that the core of the resultant vortex is circular, that the vorticity is uniformly distributed in it, and that the core volume is conserved. The amalgamation process is applied only when the rolling up of the vortex sheet is a dominant feature of the flow. The errors involved in this process are not easily evaluated and this raises doubts about its validity.

The validity of the amalgamation process becomes even more doubtful when it is applied to clusters of vortices. Several authors (for example, Sarpkaya 1975 and Clements 1973) have used it to reduce the number of discrete vortices in their two-dimensional calculations. However, for axisymmetric flows, the self-induced velocity depends strongly on the shape of the cluster and the distribution of vorticity in it. Therefore, general amalgamation should be used only when isolated and concentrated clusters are present and only far-field interactions are important.

3. Calculations and results

(a) *Oscillating disk flow*

The method was used to calculate the external flow around a plane disk of radius R which starts oscillating normal to its plane with velocity $V = \hat{V} \sin 2\pi t$, where $t = t^*/T$ is the time non-dimensionalized by the period of oscillation T. The inviscid problem depends only upon the Keulegan–Carpenter number $K = \hat{V}T/R$. The real problem, however, will also depend upon the kinematic viscosity ν and is characterized by an additional dimensionless group; either the Reynolds number $Re = 2VR/\nu$ or the frequency parameter $\alpha = R(2\pi/\nu t)^{\frac{1}{2}}$.

The choice of the time step to be used in the calculations is not straightforward. The analysis leading to equation (34) provides an upper bound on the distance between vortices, and thus the time step for an accurate representation of the self-induced velocity of the vortex sheet. Another important consideration is the accuracy with which the convection of the vortices is described. A smaller time step or, equivalently, a higher-order integration procedure increases this accuracy. Balanced against this is the time of computation, which increases as the square of the total number of vortices.

In order to determine a suitable time step, we carried out a number of identical calculations for different time steps. In one series the rolling up of a vortex formed by an impulsively started uniform flow was calculated. The results were evaluated qualitatively by observing how smoothly the vortex sheet was represented. In another series of tests the force on the disk in sinusoidal flows was calculated (as described below) for different time steps. Both the peak force and the phase of the results were compared. Surprisingly, the relatively large time step $\delta t = 0{\cdot}05$ gave smooth results which were within a few per cent of the results for the smaller time steps. This time step was chosen for the bulk of the calculations. In all of the calculations, the disk was simulated by 40 annular elements.

Figure 1 shows results of the calculation for $K = 3{\cdot}5$. A line joining two vortex rings indicates that the distance between the two sequential vortices has remained less than four times the characteristic shedding length. This was found empirically to be a good indication that that part of the vortex sheet retained an identifiable structure.

Also shown in figure 1 are the results of an experiment performed to check these calculations. A disk of 4 cm radius and 0·16 cm thick was fixed to the end of a long rod about 0·3 cm radius and oscillated sinusoidally in the centre of a circular tank, 50 cm diameter by 80 cm. The tank was filled with a saline solution in which neutrally buoyant polystyrene beads were suspended. The beads were illuminated by two collimated slit lamps (about 2 mm wide) which illuminated a plane containing the axis of symmetry normal to the camera. Particle tracks were obtained by taking photographs of relatively long exposure ($\frac{1}{25}$ s).

In comparing calculations and experiments, it must be remembered that the experimental photographs show particle tracks while the theoretical results show the instantaneous distribution of vorticity, so that they cannot be compared directly. However, the point vortices also serve as fluid markers and the experimental results do give a qualitative indication of the location of the primary vorticity. In this qualitative sense, the results agree quite well.

Calculations and experiments were carried out for oscillations with $K \sim O(1)$. In

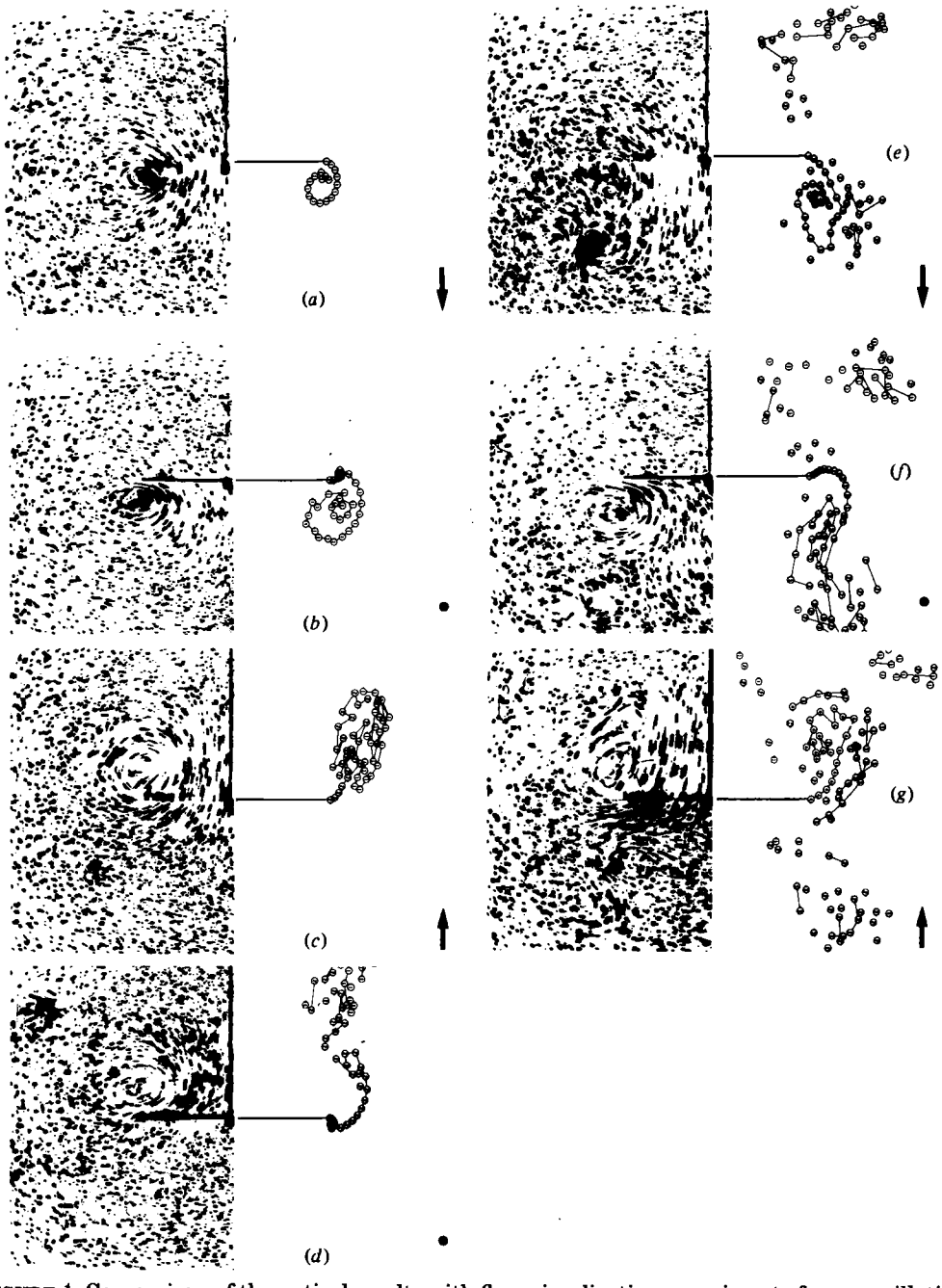

FIGURE 1. Comparison of theoretical results with flow visualization experiments for an oscillating disc starting from rest. $K = 3{\cdot}5$, $Re = 11\,200$, $\delta t = 0{\cdot}0525$. ↑ is the velocity at infinity. (*a*) $t = \frac{1}{4}$, (*b*) $\frac{1}{2}$, (*c*) $\frac{3}{4}$, (*d*) 1, (*e*) $\frac{5}{4}$, (*f*) $\frac{3}{2}$, (*g*) $\frac{7}{4}$.

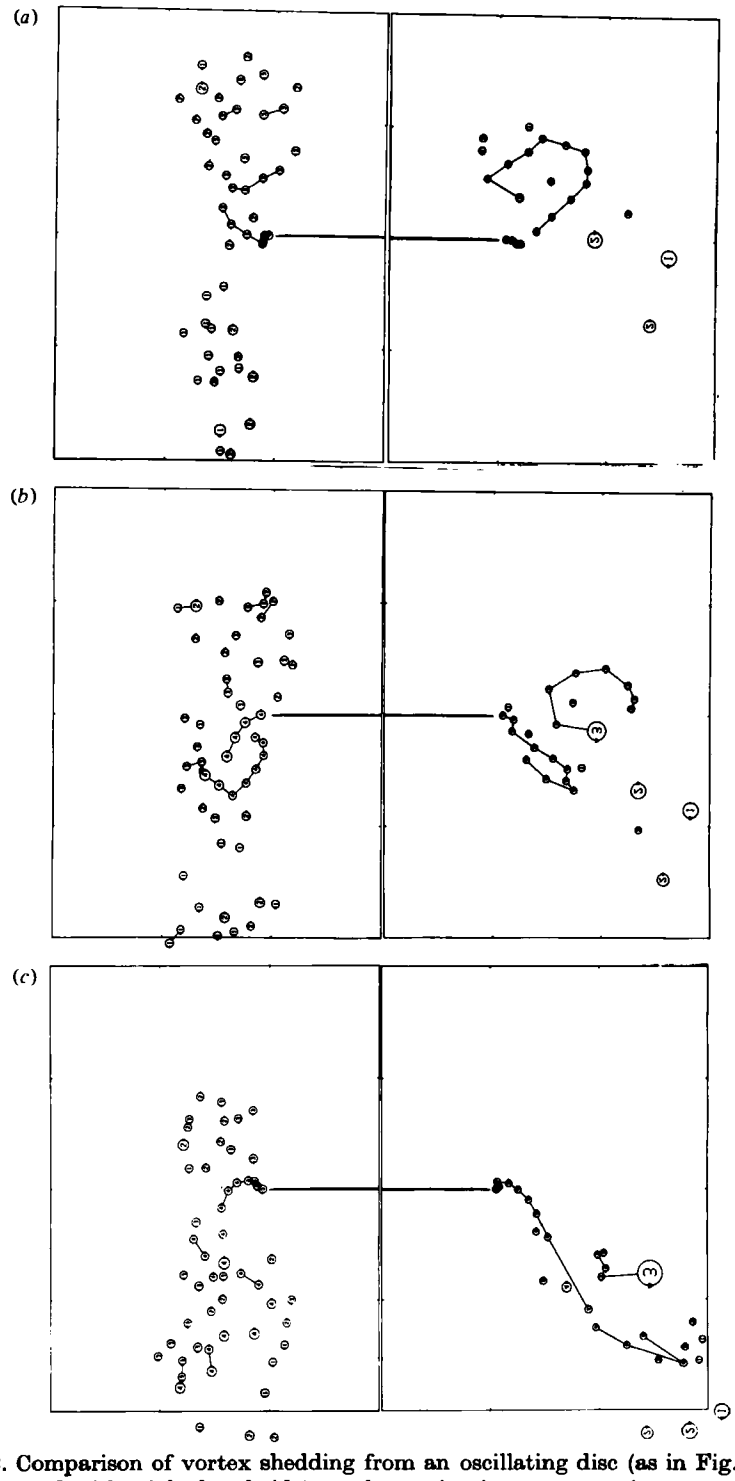

FIGURE 2. Comparison of vortex shedding from an oscillating disc (as in Fig. 1) without (left-hand side) and with (right-hand side) amalgamation into core vortices. (a) $t = \frac{3}{2}$, (b) $\frac{7}{4}$, (c) 2.

this range, the displacement of particles in the undisturbed flow is comparable to the scale of the body. It is, therefore, impossible for the large-scale rolled-up vortices to move far from the edge of the body from which they are shed except by their self-induced velocity and, more importantly, by the induced velocity field of the other such vortices.

One feature of the theoretical predictions which was subsequently observed in the experiments is the formation of vortex pairs and their *unidirectional* convection away from the disk. The vorticity shed during the first half-cycle tends to roll up into a single vortex ring. As the free stream slows down, the flow at the edge of the disk reverses and a second vortex sheet of opposite sign starts and continues to be shed during the second half of the cycle. Meanwhile, the first vortex is convected around the disk by both its self-induced velocity and by the reversed free stream. This vortex interacts with part of the second vortex sheet to form a vortex pair which moves away from the disk. The residual of the second vortex sheet is neither as strong nor as organized as the first vortex and so that when the flow again reverses at the start of the second cycle it does not interact very strongly with the third vortex. This third vortex sheet develops into an organized vortex ring very much like the first one and the process is repeated in succeeding cycles.

Behaviour similar to that predicted by the calculations was observed in the experiments. An asymmetric wake whose direction depended only on the starting direction of the flow was certainly established and seemed to be quite stable. The flow remained axisymmetric up to a distance of about one diameter from the disk. Because of diffusion and possibly instabilities of the vortices it was difficult to follow their motion at greater distances. Also, because the tank was relatively small, a secondary motion was rapidly established which also obscured the long-term motion of the vorticity.

The pattern of flow around the oscillating disk is closer to that observed for a single, two-dimensional edge (Graham 1980) than to that of a two-dimensional body with two edges (Singh 1979). In the latter case the vorticity from one edge tends to migrate around the body to join with the vortex of the same sign growing on the opposite edge. This process appears to revolve around the body with the vortex pairs convecting away from the edges at an angle of about 45°. Because of the axisymmetry of the disk flow, this cannot happen.

Figure 2 shows the comparison between two calculations. They are for the same case and the same relatively large time step, $\delta t = 0{\cdot}0875$. On the left, the vortex rings have not been amalgamated; on the right, an amalgamation procedure has been used. In general, the gross features of the flow, such as the predicted centres of circulation, are similar in both cases. However, amalgamation does seem to obliterate the finer features of the flow and is, therefore, less satisfactory.

Once the vorticity and hence the velocity distribution has been calculated, equation (4) can be used to calculate the pressure field. The unsteady axial force acting on the disk is

$$F(t) = \int_S p(S', t)\, dS', \tag{40}$$

where S represent the entire surface of the disk. It is convenient to consider this unsteady force as arising from two contributions; one associated with the inertial

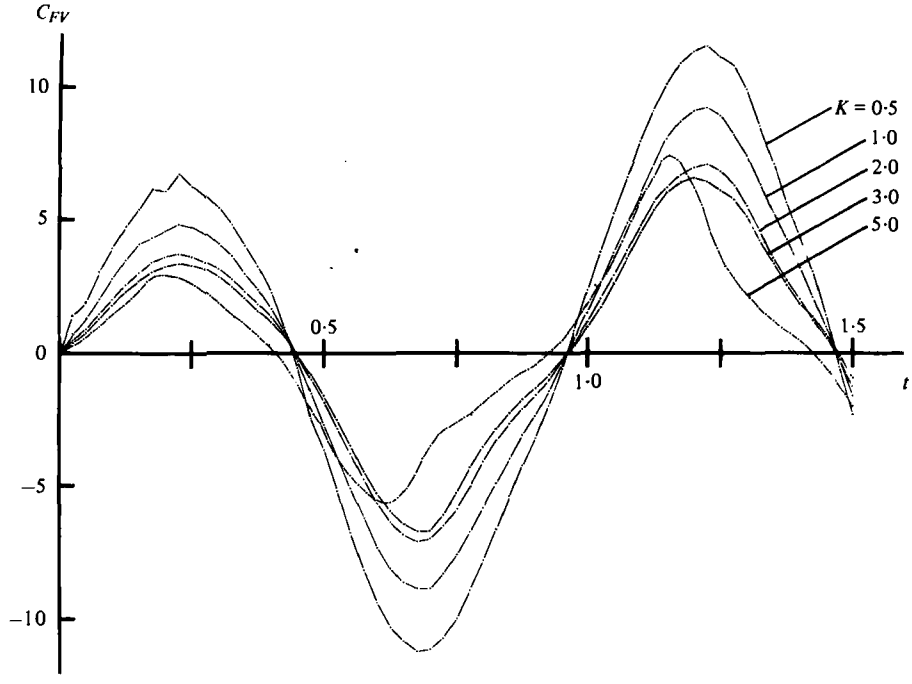

FIGURE 3. The vortex force coefficient for a disk in oscillatory flow starting from rest.

force occurring for attached flow around the disk and the other from the shedding of vorticity. We therefore write (Graham 1980)

$$F(t) = \tfrac{4}{3}\pi\rho\hat{V}R^3C_{M0} + \tfrac{1}{2}\pi\rho\hat{V}^2R^2C_{FV}(t); \tag{41}$$

C_{M0} is the attached flow inertia coefficient based on a sphere of equal radius and has a value of 0·637 and C_{FV} is the vortex force coefficient, non-dimensionalized by the area of the disk.

Figure 3 shows a plot $C_{FV}(t)$ calculated for the first $1\frac{1}{2}$ cycles starting from rest, for different values of K. The amplitude decreases with increasing K and the zero crossing points are remarkably constant up to a value of K of about 3. The peak amplitude of the first half-cycle is low because during this period only one vortex has been shed. After this the peak amplitudes remain fairly constant.

Equation (41) can be written in the form of Morison's equation

$$F(t) = \tfrac{4}{3}\pi\rho\dot{V}R^3C_M + \tfrac{1}{2}\pi\rho V|V|R^2C_D, \tag{42}$$

where

$$C_M = C_{M0} + \frac{3K}{4\pi}\int_0^1 C_{FV}(t)\cos 2\pi t\,dt \tag{43}$$

and

$$C_D = \frac{3\pi}{4}\int_0^1 C_{FV}(t)\sin 2\pi t\,dt. \tag{44}$$

For very small values of K, the vortex shedding close to the disk should be similar to that for a single plane edge. For this case we expect (Graham 1980) that $C_D = AK^{-\frac{1}{2}}$ and $C_M - C_{M0} = BK^{\frac{1}{2}}$, where A and B are fixed coefficients. Figure 4 shows the

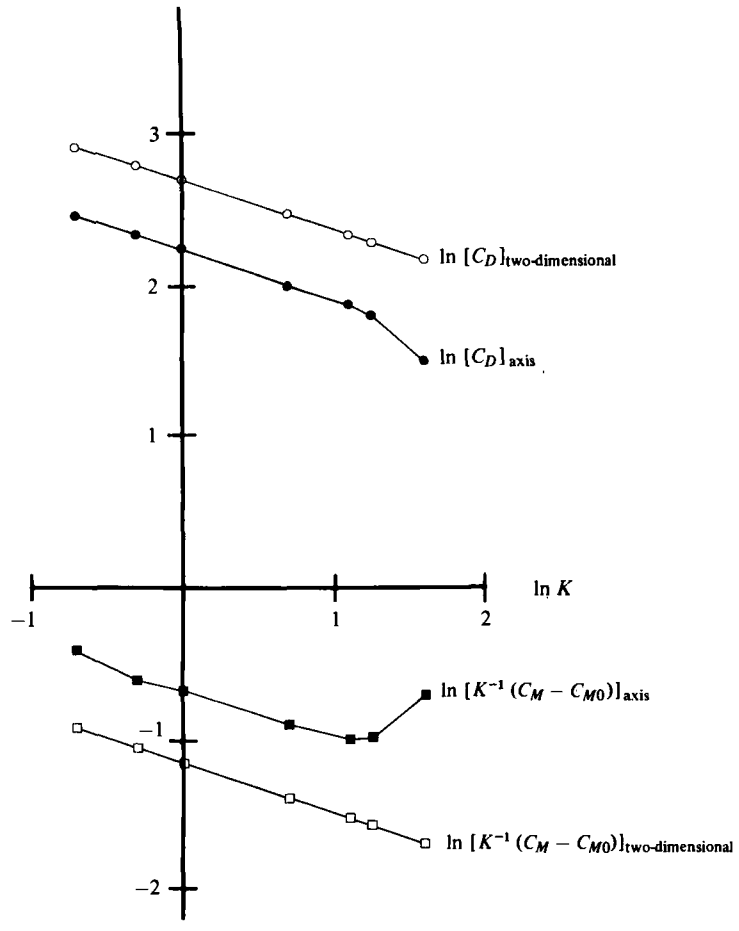

FIGURE 4. The variation of drag and inertia coefficients with Keulegan–Carpenter number for a disk and an isolated two-dimensional edge.

calculated values of C_D and $(C_M - C_{M0})K^{-1}$ together with the values for a single edge. We see that the results for the disk follow the $K^{-\frac{1}{2}}$ behaviour predicted for a single edge up to a value of K of about 3; above this value they diverge rapidly.

(*b*) *Oscillating orifice flow*

For the second application of our point-vortex calculation procedure we chose a flow which is similar in many ways to those which stimulated this research; internal oscillatory flow through a circular pipe with a flat plate orifice in the middle. An onset flow $V = \hat{V} \sin 2\pi t/T$ was imposed. The pipe of radius R and orifice of radius r_0 were simulated by 80 annular elements distributed over a length of 12 pipe radii on either side of the orifice. The governing parameters for the calculation are the Keulegan–Carpenter number $K = \hat{V}T/R$ and a parameter describing the relative size of the orifice. Following clinical medical practice, the orifice size is expressed by the constriction ratio; i.e. the fraction of pipe area blocked by the orifice, $c = 1 - (r_0/R)^2$. In this case the theory has been developed for infinite Reynolds number. Viscosity has the additional effect in internal flows of influencing the incident flow profiles. In

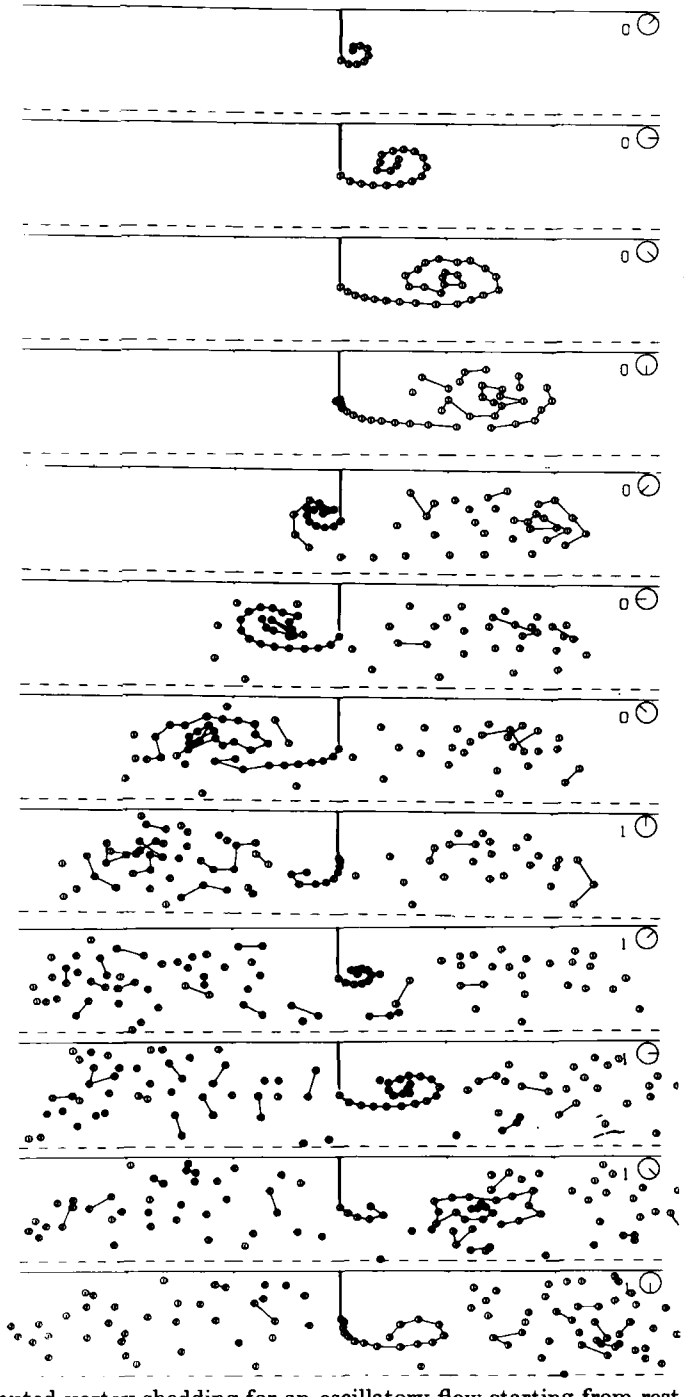

FIGURE 5. Computed vortex shedding for an oscillatory flow starting from rest through a 70% constricted orifice plate in a pipe. $K = 6{\cdot}0$, $\delta t = 0{\cdot}039$. Results are shown at every $\frac{1}{8}$ cycle.

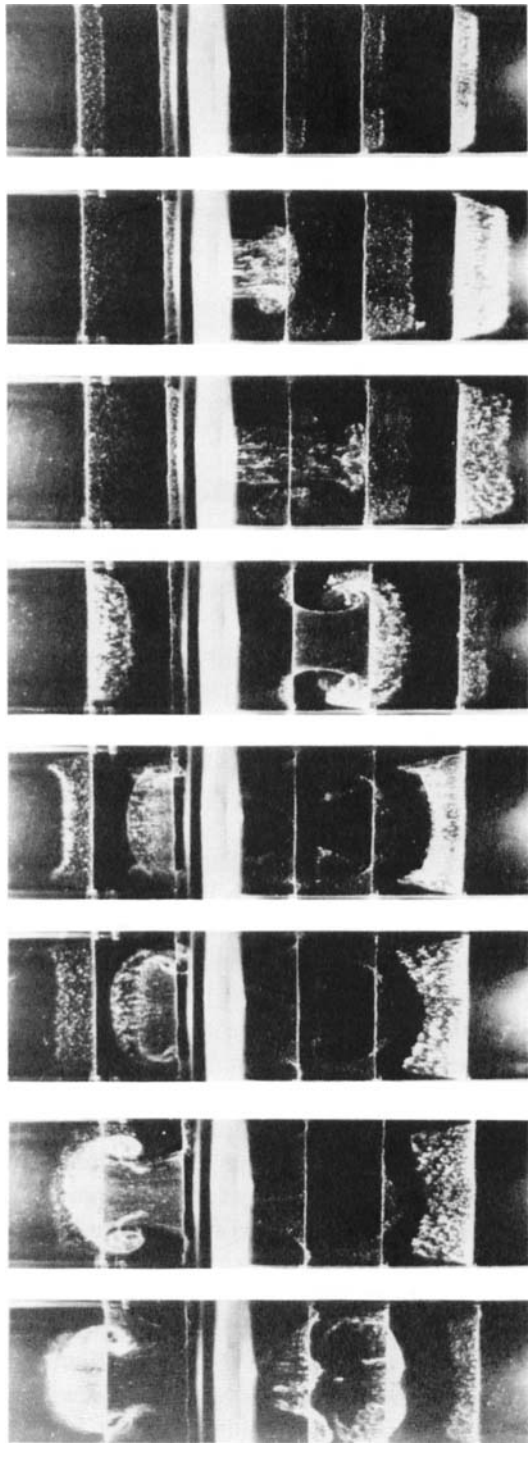

FIGURE 6. Flow visualization experiments for an oscillatory flow started from rest through a 70% constricted orifice plate in a pipe. $K = 6{\cdot}0$, $Re = 485$. Results are shown at every $\frac{1}{8}$ cycle.

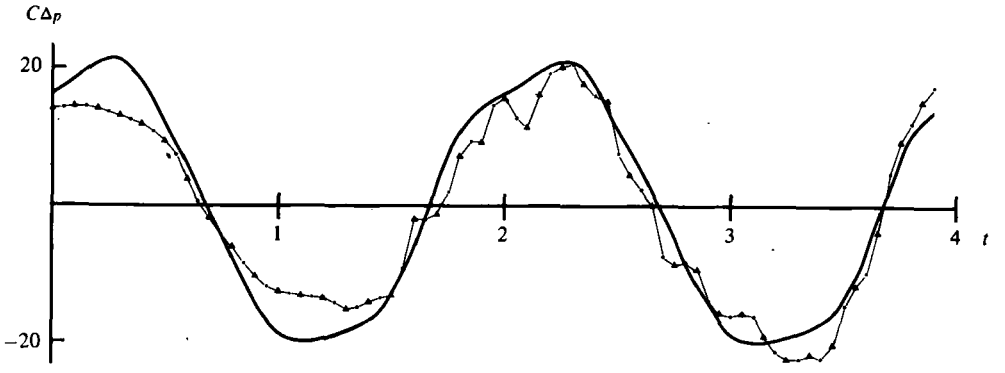

FIGURE 7. Computed (▲- · -▲) and measured (——) pressure difference coefficients across a 70% constricted orifice plate in oscillatory flow started from rest. $K = 6{\cdot}0$, $Re = 485$.

purely oscillatory flow the thickness of the Stokes layer or the pipe walls scales as $(\nu T)^{\frac{1}{2}}$. With significant mean flow, the thickness of the affected layer will also depend upon the entry length of the pipe. In either case, if the boundary-layer thickness is significant, the calculations presented here for a flat incident flow profile will not apply.

Calculations were carried out for a number of cases for which flow visualization and pressure drop measurements were available (Djilali 1978). Figure 5 shows the results of numerical calculations for $K = 6{\cdot}0$ and $c = 70\,\%$ and the same time step as was used in the disk calculations, $\delta t = 0{\cdot}05$. The strength of each vortex ring varies, of course, depending upon the conditions when it was originally shed. But each vortex does serve as a fluid marker.

Figure 6 shows the results of a flow visualization experiment, using the hydrogen bubble technique for the same conditions as figure 5 in a pipe of 25 mm diameter. The period of oscillation in the experiment T was 4 s, which means that the Reynolds number based on pipe diameter $Re = 486$ and the thickness of the Stokes layers ~ 2 mm. Again the theoretical results cannot be compared directly with the experimental results which, in this case, record the convection of streak tracks. However, the location of the major centres of circulation can be estimated from the experimental results and they correspond well with the theoretical predictions.

The primary difference between orifice and disk flow is that the self-induced velocity of the vortex rings, formed by the rolling up of the vortex sheet shed by the orifice, convects them away from the orifice. This effect is opposed by the 'images' in the bounding pipe walls, and therefore the ratio of the radius of the vortex to that of the pipe is important. As a result we see that very little of the vorticity generated during each half-cycle is conducted back through the orifice particularly in large blockage ratios. Most of it remains on the side of the orifice where it was generated. In the experiments it is dissipated by diffusion. In the calculations it does not dissipate but does disperse due to interactions with other vortices and with the wall. In our calculations this dispersion led to strong interactions with the bound vortices representing the walls and as the free vortices approached the end of the simulated pipe instabilities developed.

Another difference between orifice and disk flow is how the flow in the neighbour-

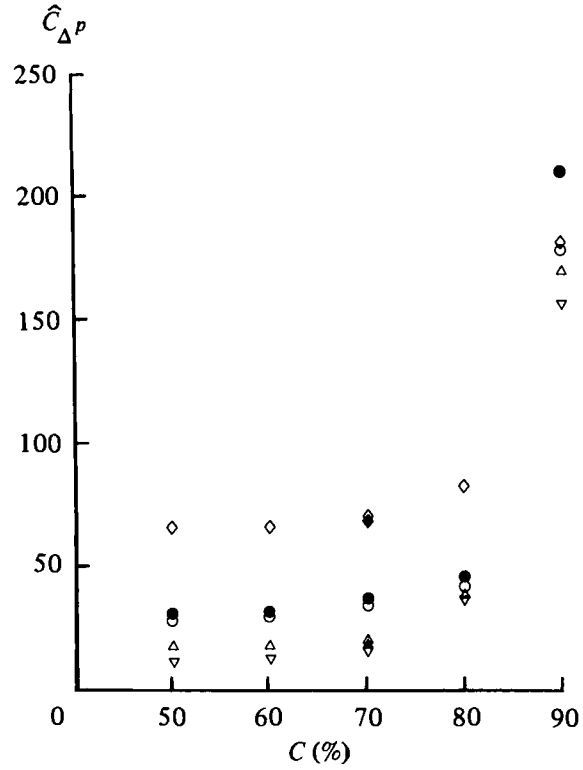

FIGURE 8. Computed and measured peak pressure difference coefficients across orifice plates with various constriction ratios. Experimental: ◇, K = 2·47; ○, 4·95; △, 7·42; ▽, 9·89. Theoretical: ◆, K = 2·47; ●, 4·72; ▲, 7·42.

hood of the edge is affected by the evolving vortex sheet. In both cases the velocity at the edge induced by the vortex sheet is opposite to the free-stream velocity. As a result, the flow at the edge and hence the shedding tends to reverse before the onset flow reverses. In the orifice, however, this effect is counteracted by the self-induced velocity which acts with the incident velocity and the shedding reverses almost exactly in phase with the onset flow.

The pressure distribution along the walls of the pipe can be calculated by using equation (4) on the streamline at the wall. Defining the pressure coefficient

$$C_p(s,t) = [p(s,t) - p(\infty,t)]/\tfrac{1}{2}\rho\hat{V}^2,$$

the pressure drop coefficient between two points, s_1 and s_2, is simply

$$C_{\Delta p}(s_1, s_2, t) = \frac{V_\tau^2(s_2,t) - V_\tau^2(s_1,t)}{\hat{V}^2} + \frac{2}{\hat{V}}\int_{s_1}^{s_2} \frac{\partial V_\tau(s',t)}{\partial t}\,ds' + \frac{\partial \Delta\phi_e}{\partial t}, \tag{45}$$

where s is the distance along the wall including the orifice and the last term is the contribution of the vortex sheet shed at the edge. Figure 7 shows the calculated and experimentally measured values of $C_{\Delta p}$ when the pressure measuring points are 3 pipe diameters either side of the orifice and c = 70 %, K = 6·0 and Re = 485. The asymmetry of the experimental results is due to a slight bevelling of the edge of the orifice.

This was easily demonstrated by reversing the orifice plate and indicates the sensitivity of separated flows to the detailed nature of the separating edge. The agreement between theory and experiment is satisfactory and confirms the power of the method to predict the global features of the flow.

In agreement with other workers' observations (Young & Tsai 1973*a*, *b*; Clark 1976*a*, *b*) the experimental peak pressure-drop coefficient, $\hat{C}_{\Delta p}$, was found to be relatively independent of c for c less than about 70% and then to increase very rapidly with c; $\hat{C}_{\Delta p}$ was also found to be relatively independent of Re over the range tested ($318 \leqslant Re \leqslant 1272$) but did vary with K. These results are shown in figure 8 along with the theoretically predicted $\hat{C}_{\Delta p}$. The agreement between theory and experiment is excellent until $c = 90\%$. This disagreement at $c = 90\%$ is not surprising, first because the flow was observed experimentally to be turbulent over most of the cycle and second because the assumptions leading to the use of the two-dimensional shedding theory and of negligible self-induced velocity are not valid for such large constrictions.

4. Conclusions

The method of discrete vortices, previously used to calculate two-dimensional flows, has been extended to axisymmetric flows. It is a relatively fast method for calculating unsteady, high-Reynolds-number separated flow. By comparing our numerical predictions with experimental results, we conclude that the method predicts the dominant features of the flow accurately. In unbounded oscillatory flow around a disk, it correctly predicts the pairing and the unidirectional streaming of the shed vortex rings. In bounded oscillatory flow through an orifice, it correctly predicts the location of the vortices which are shed during each half-cycle and, more importantly, it correctly predicts the magnitude of the pressure drop across the orifice.

REFERENCES

Anton, L. 1939 Ausbildung eines Wirbels an der Kante einer Platte. *Ingenieur-Archiv* **10**, 411–421. (English Translation, 1956, *N.A.C.A.* TM-1398.)

Ashurst, W. T. 1979 Piston-cylinder fluid motion via vortex dynamics. Presented at *Euromech* 119, *London*.

Caro, C. G., Fitzgerald, J. M. & Schroter, R. S. 1971 Atheroma and arterial wall shear stress. *Proc. Roy. Soc.* B **177**, 109–159.

Chaplin, H. R. 1964 A method for numerical calculation of slipstream contraction of a shrouded impulse disk in the static case with application to other axisymmetric potential flow problems. *David Taylor Model Basin Rep.* no. 1857.

Clark, C. 1976*a* The fluid mechanics of aortic stenosis. I. Theory and steady flow experiments. *J. Biomech.* **9**, 521–528.

Clark, C. 1976*b* The fluid mechanics of aortic stenosis. II. Unsteady flow experiments. *J. Biomech.* **9**, 567–573.

Clements, R. R. 1973 An inviscid model of two-dimensional vortex shedding. *J. Fluid Mech.* **57**, 321–336.

Clements, R. R. & Maull, D. J. 1975 The representation of sheets of vorticity by discrete vortices. *Prog. Aerospace Sci.* **16**, 129–146.

Davies, P. O. A. L. & Hardin, J. C. 1974 Potential flow modelling of unsteady flow. In *Numerical Methods in Fluid Mechanics* (ed. C. A. Brebia & J. J. Connor), pp. 42–64. London: Pantech Press.

DIDOLEN, N. 1979 On the formation of vortex rings: rolling up and production of circulation. *Z. angew. Math. Phys.* **30**, 101–116.

DJILALI, N. 1978 Oscillatory flow through a sharp-edged orifice plate. M.Sc. thesis, Imperial College, Dept of Aeronautics.

EVANS, R. A. & BLOOR, M. I. G. 1976 The starting mechanism of wave-induced flow through a sharp-edged orifice. *J. Fluid Mech.* **82**, 115–128.

FAGE, A. & JOHANSEN, F. C. 1927 The structure of the vortex sheet. *Phil. Mag.* **5** (7), 417–436.

FINK, P. T. & SOH, W. K. 1974 Calculations of vortex sheets in unsteady flow and applications in ship hydrodynamics. *10th Symp. Naval Hydrodynamics, Cambridge, Mass.*, pp. 463–489.

FRY, D. L. 1973 Response of the arterial wall to certain physical factors in atherogenesis. Ciba Foundation Symposium 12. *Excerpta Medica*, 93–125.

GIESING, J. P. 1969 Vorticity and Kutta condition for unsteady multienergy flows. *Trans. A.S.M.E.* E, *J. Appl. Mech.* **36**, 608–613.

GRAHAM, J. M. R. 1977 Vortex shedding from sharp edges. *Imperial College Aero. Rep.* 77–06.

GRAHAM, J. M. R. 1980 The forces on sharp-edged cylinders in oscillatory flow at low Keulegan–Carpenter numbers. *J. Fluid Mech.* **97**, 331–346.

HESS, J. L. & SMITH, A. M. O. 1966 Calculations of potential flow about arbitrary bodies. *Prog. Aero. Sci.* **8**.

KNOTT, G. F. & MACKLEY, M. R. 1980 On eddy-motions near plates and ducts, induced by water waves and periodic flows. *Proc. Roy. Soc.* (in press).

LAMB, H. 1957 *Hydrodynamics*, 6th edn, pp. 202–249. Cambridge University Press.

MANGLER, K. W. & SMITH, J. H. 1956 A theory of slender delta wing with leading edge separation. *R.A.E. Rep.* 2442.

MATES, R. E., GUPTA, R. L., BELL, A. C. & KLOCKE, F. J. 1978 Fluid dynamics of coronary artery stenosis. *Circulation Res.* **42**, 152–162.

MOORE, D. W. 1974 A numerical study of the roll-up of a finite vortex sheet. *J. Fluid Mech.* **63**, 225.

PRANDTL, L. 1924 Über die Entstehung von Wirbeln in der idealen Flüssigkeit. *Vorträge aus dem Gebiete der Hydro- und Aerodynamik, Innsbruck*, 1922 (ed. von Kármán & Levi-Civita). Springer.

ROSENHEAD, L. 1931 The formation of vortices from a surface of discontinuity. *Proc. Roy. Soc.* A **134**, 170–192.

SAFFMAN, P. G. 1978 The number of waves on unstable vortex rings. *J. Fluid Mech.* **84**, 625–639.

SARPKAYA, T. 1975 An inviscid model of two-dimensional vortex shedding for transient and asymptotically separated flow over an inclined plate. *J. Fluid Mech.* **68**, 109–128.

SARPKAYA, T. & SCHOAFF, R. L. 1979 Inviscid model of two-dimensional vortex shedding by a circular cylinder. *A.I.A.A. J.* **17**, 1193–1200.

SINGH, S. 1979 Forces on bodies in an oscillatory flow. Ph.D. thesis, University of London.

SMITH, A. M. O. & PIERCE, J. 1958 Exact solution of the Neumann problem – calculation of plane and axially symmetric flows about or within arbitrary boundaries. *Douglas Aircraft Co.* Rep. 26988.

TOMM, D. 1977 Model investigation of sound generation in vessel stenosis. *INSERM – Euromech 92, Cardiovascular and pulmonary dynamics* **71**, 179–192.

WEDERMEYER, E. 1961 Ausbildung eines Wirbelpaares an den Kanten einer Platte. *Ingenieur-Archiv* **30**, 187–200.

YOUNG, D. F. 1979 Fluid mechanics of arterial stenoses. *J. Biomech. Engng* **101**, 157–175.

YOUNG, D. F. & TSAI, F. Y. 1973*a* Flow characteristics in models of arterial stenoses. *J. Biomech.* **6**, 395–410.

YOUNG, D. F. & TSAI, F. Y. 1973*b* Flow characteristics in models of arterial stenoses. *J. Biomech.* **6**, 547–559.